HHS Public Access

Author manuscript

Phys Med Biol. Author manuscript; available in PMC 2020 April 21.

Published in final edited form as:

Phys Med Biol. ; 64(17): 175016. doi:10.1088/1361-6560/ab31e3.

Electronics method to advance the coincidence time resolution with bismuth germanate

Joshua W Cates[1,3], **Craig S Levin**[2]

[1]Applied Nuclear Physics, Lawrence Berkeley National Laboratory, Berkeley, CA, United States of America

[2]Stanford University School of Medicine, Stanford, CA, United States of America

[3]Author to whom any correspondence should be addressed.

Abstract

Exploiting the moderate Cherenkov yield from 511 keV photoelectric interactions in bismuth germanate (BGO) scintillators enables one to achieve a level of coincidence time resolution (CTR) appropriate for time-of-flight positron emission tomography (TOF-PET). For this approach, owing to the low number of promptly emitted light photons, single photon time resolution (SPTR) can have a stronger influence on achievable CTR. We have previously shown readout techniques that reduce effective device capacitance of large area silicon photomultipliers (SiPMs) can yield improvements in single photon response shape that minimize the influence of electronic noise on SPTR. With these techniques, sub-100 ps FWHM SPTR can be achieved with 4×4 mm^2 FBK near-ultra-violet high density (NUV-HD) SiPMs. These sensors are also useful for detecting Cherenkov light due to relatively high photon detection efficiency for UV light. In this work, we measured CTR for BGO crystals coupled to FBK NUV-HD SiPMs with a passive bootstrapping readout circuit that effectively reduces the SiPM device capacitance. A range of CTR values between 200 ± 3 and 277 ± 7 ps FWHM were measured for $3 \times 3 \times 3$ and $3 \times 3 \times 15$ mm^3 crystals, respectively. This readout technique provides a relatively simple approach to achieve state-of-the-art CTR performance using BGO crystals for TOF-PET.

Keywords

time-of-flight PET; positron emission tomography; bismuth germanate

1. Introduction

Methods for continuing to improve CTR for TOF-PET with scintillators include exploiting small populations of promptly emitted light photons (Lecoq *et al* 2014, Gundacker *et al* 2016a, Lecoq 2017). These methods focus on the detection of prompt signatures (hot intra-band luminescence, Cherenkov light, and/or others) from 511 keV photon interactions that are generated much faster than the scintillator's dominant luminescence yield. In particular, the detection of Cherenkov light has received a significant amount of investigation for the

jcates@lbl.gov.

development of TOF-PET detectors with fast timing capabilities. Relative to luminescence processes that have tens-to-hundreds of nanoseconds intrinsic decay time constants, this process is essentially instantaneous. Therefore, there is potential to use this promptly emitted light to derive an estimate for 511 keV photon interaction time with lower temporal variance.

Among the interesting candidate crystals to explore for this approach is BGO. BGO was a standard material used in PET systems for decades, eventually being replaced with lutetium oxyorthosilicate (LSO) scintillators for improved timing and energy performance. However, BGO is much lower cost. In bulk quantity, BGO can be 4-to-5 times less expensive than LSO. It also has higher 511 keV photon interaction probability and photoelectric fraction for equivalent crystal lengths. Due to BGO's higher index of refraction, 511 keV photoelectrons also produce more Cherenkov light than LSO scintillators (~20 above BGO's absorption band and ~9 above LSO's absorption band (Brunner and Schaart 2017)), and its ~300 nm absorption band also allows it to be more transmissive to UV light. Two recent studies have shown very promising progress towards using BGO in lower cost TOF-PET detectors comprising analog and digital SiPMs by exploiting it is moderate Cherenkov yield (Kwon *et al* 2016a, Brunner and Schaart 2017). In Brunner and Schaart (2017), it was shown that Philips DPC-3200 digital SiPMs (Liu *et al* 2016) with the ability to provide a timestamp from the first detected light photon can yield ~400 ps FWHM CTR for 20 mm length BGO crystals at room temperature. In Kwon *et al* (2016a), 562 ps FWHM was achieved for 20 mm length BGO crystals coupled to FBK NUV-HD (Piemonte *et al* 2016) SiPMs using leading edge time pickoff. Therefore, it is feasible to develop TOF-capable PET detector modules using existing photosensor technologies coupled to BGO crystals having lengths that provide adequate photon detection efficiency for clinical PET. This creates opportunities to design more economical TOF-PET detector modules.

TOF-PET detectors that employ a mixture of Cherenkov and luminescence photons in order to estimate 511 keV photon time of interaction have two unique challenges to optimizing achievable timing performance: (1) CTR is more sensitive to SPTR of the SiPM and associated electronic readout used (Gundacker *et al* 2016a) and (2) the optimum leading edge threshold is well below 1 light photon equivalent level (Gundacker *et al* 2016b), where the lowest achievable threshold above the noise floor yields optimum CTR. Therefore, in order to optimize the CTR of these detector types, single photon response shape (its rise above the noise) and SPTR should also be optimized. For relatively fast and bright inorganic scintillation materials with luminescence kinetics similar to LSO, SPTR has a weaker influence on CTR (Gundacker *et al* 2013, Cates *et al* 2015). In those cases, significant improvements in SPTR yield minor improvements in CTR. In addition, the optimum threshold for these detectors (typically 1–2 photon equivalent or higher) yields less susceptibility to single photon response shape, i.e. the amplitude of single photon pulses does not need to be substantially higher than noise level to optimize the leading edge threshold. However, in order to extract excellent CTR from detectors that exploit a small population of prompt signatures to estimate 511 keV photon interaction time, front end signal processing and SiPM performance that provides improved SPTR and single photon response shape is beneficial.

We have previously shown the application of readout techniques that reduce effective device capacitance (Kwon *et al* 2015, Zhang and Schmand 2016, Kwon *et al* 2016b) of large area SiPMs can yield improvements in single photon response shape, minimizing the influences of electronic noise on SPTR Cates *et al* (2018a). With this readout technique, ≤100 ps FWHM SPTR can be achieved for large area FBK NUV-HD SiPMs (>4 × 4 mm^2 active area). These sensors are also useful for detecting Cherenkov light due to high photon detection efficiency for UV light. Therefore, this electronic readout technique with UV sensitive SiPMs is a promising approach for improving CTR with BGO-based detectors. In this work, we measured achievable CTR for BGO crystals of various lengths using FBK NUV-HD SiPMs with a passive capacitance compensation readout circuit that effectively improves the SPTR. We believe these results will be of particular interest to TOF-PET system developers looking for a low cost solution to achieve <300 ps CTR.

2. Experimental materials and methods

2.1. Bootstrapping circuit

A passive capacitance compensation circuit was assembled, which is a modified version of that outlined in Zhang and Schmand (2016), where a balun transformer is connected between the cathode and anode of the SiPM in a balanced-to-unbalanced configuration to two Minicircuits MAR-6 RF amplifiers (Minicircuits 2019) in cascade (Cates *et al* 2018a). A simple schematic of the circuit is shown in figure 1(a). The balun transformer used in the circuit is a Macom MABA-007159 (MACOM 2019) (50 Ω impedance and 1:1 turn ratio). Also shown in figure 1(c) is the average of 700 single photon pulses from a 3 × 3 mm^2 Hamamatsu S13360 biased at 58.5 V using the circuit seen in figure 1(b), as an example of single photon pulse shape with and without the balun transformer in place (the two average pulses are offset in time in figure 1(c) for clarity). One important note is that the balanced-to-unbalanced connection of the transformer to the SiPM should result in 2-fold increase in pulse amplitude. The observed factor of ~3.5 improvement in single photon pulse amplitude shown in figure 1(b) suggests an additional boost from a lower effective terminal capacitance, as described in Zhang and Schmand (2016).

2.2. Coincidence time resolution measurement

A simple coincidence timing setup (Cates and Levin 2016) was used to measure CTR for BGO crystals of various lengths. Crystal elements of 3 × 3 × 3, 3 × 3 × 5, 3 × 3 × 10, and 3 × 3 × 15 mm^3 in size, with mechanically polished surfaces, were wrapped in Teflon tape. Crystals were optically coupled to 4 × 4 mm^2 FBK NUV-HD SiPMs with 40 × 40 μm^2 Geiger cell size (Piemonte *et al* 2016). Sensors were read out with the circuit shown in figure 1(b). Cathode signals were split with a 20/80% ratio using a resistive divider for the energy and timing channels, respectively. Raw waveforms from the detectors were digitized by an Agilent DSO940 2 GHz oscilloscope. Coincidence processing was performed using software on the oscilloscope. Events with energies falling within the FWTM of the 511 keV photon photopeak for both detectors were processed. Leading edge discrimination was used to estimate time of interaction in post processing of digitized waveforms, and the influence of baseline offset from dark pulses and cross talk events was corrected by averaging a one nanosecond (ns) region of the baseline in front of each pulse (Vinke *et al* 2009, Seifert *et al*

2009, Schaart *et al* 2010). The measured CTR distributions for BGO were fit with a Lorentzian function, as Kwon *et al* (2016a) and Brunner and Schaart (2017) demonstrated the distributions exhibit long tails best described by a Lorentzian curve. The FWHM and FWTM of these distributions were taken from the fitted curve. All experiments were performed at room temperature with no active cooling.

2.3. CTR with signal processing for simple leading edge time pickoff

In the methods outlined in section 2.2, 511 keV photon time of interaction was estimated from leading edge time pickoff that was corrected for baseline shifts due to Geiger discharges prior to the onset of the pulse's rising edge. However, real leading edge discriminators using discrete electrical components require high frequency filtering of signals to minimize the influence of these baseline shifts (Gola *et al* 2013). While this approach optimizes a leading edge timing estimator in the presence of dark counts, this filtering can reduce signal amplitude and amplify high frequency noise. In order to determine the achievable CTR with the BGO crystals in this scenario, we also performed digital high pass filtering on the digitized waveforms using a rational transfer function with parameters varied for different high pass filters and estimated 511 keV photon time of interaction from simple leading edge time pickoff (i.e. no digital baseline corrections were performed). The pass frequency of the filter was varied to determine if there was an optimum setting.

3. Results

3.1. Coincidence time resolution

CTR with BGO crystals 3, 10, and 15 mm in length as a function of SiPM bias is shown in figure 2(a). The measured CTR at optimum sensor bias and leading edge threshold were 200 $\pm$ 3, 218 $\pm$ 4, 269 $\pm$ 7, and 277 $\pm$ 7 ps FWHM, respectively. Measured CTR versus leading edge threshold is shown for each crystal size, at optimum SiPM bias in figure 2(b).

An example of a CTR distribution for 3 $\times$ 3 $\times$ 3 mm^3 BGO crystals in coincidence at 39V and optimum leading edge discriminator threshold is shown in figure 3(a). As previously demonstrated in Kwon *et al* (2016a) and Brunner and Schaart (2017), the distribution exhibits long tails that makes it best described by a Lorentzian curve. Therefore, it is also important to quantify the tails of the distribution when relating measured CTR to TOF-PET. Figure 3(b) shows the measured CTR in FWHM and FWTM for each crystal length, with optimum SiPM bias and leading edge threshold.

3.2. CTR distribution analysis

Due to the tails of the CTR distributions for measured data in section 3.1, it is important to quantify both their potential effect on effective detector sensitivity based on coincidence time window width and differences between the observed distributions and a standard Gaussian kernel. Specifically, the FWTM of the observed distributions and the percentage of events lying outside a standard Gaussian timing kernel were calculated. Figure 4(a) shows the cumulative distribution function (CDF) for each crystal length with optimum measurement settings, and the percentage of events falling within set coincidence window

widths is shown in figure 4(b). For figure 4(a), a cumulative probability 1 represents all measured coincidence data, and in figure 4(b) 'percentage of events' on the *x*-axis refers to the percentage of measured coincidence events that fall within a coincidence window with a width defined on the *y*-axis.

Figure 5 shows the CTR distribution for 15 mm length crystals in coincidence with both Lorentzian and Gaussian fits. The percentage of coincidence counts extending beyond a standard Gaussian coincidence timing fit was quantified as 17.7%. This was quantified by integrating all observed coincidence events beyond the 6σ bounds of the Gaussian fit to the data shown in figure 5.

3.3. CTR with high pass filtering and simple leading edge time pickoff

The CTR at FWHM for 15 mm length BGO crystals with the SiPMs operated at 40 V is shown in figure 6 as a function the time constant of the high pass filter on the digitized waveforms from the detectors. The time constants range from 0.1–6.25 nanoseconds (ns). With proper filtering, the same CTR achieved with digital baseline corrections, indicated by the red line, is achieved with a simple leading edge timing estimators, within experimental error. A range of time constants, ~0.5–2 ns, provided optimum performance, which translate to equivalent capacitor values in the 10's of picoFarads for a 50 Ohm impedance line.

4. Discussion

We have presented CTR studies for BGO crystals coupled to UV-sensitive SiPMs with electronic readout that provides excellent SPTR. CTR of 200 $\pm$ 3, 218 $\pm$ 4, 269 $\pm$ 7, and 277 $\pm$ 7 ps FWHM was measured for BGO crystals in coincidence having 3, 5, 10, and 15 mm length, respectively. Consistent with other works that report CTR values for crystals that emit a moderate amount of Cherenkov light in addition to a luminescence yield, optimum threshold for leading edge time pickoff is well below the single photon equivalent amplitude, and just above baseline noise. This highlights another benefit of the electronic readout presented in section 2.1 for coincidence timing measurements with BGO scintillators. As shown in figure 1, the improved single photon response shape provided by the bootstrapping readout circuits can boost this optimum point for leading edge discriminators above the noise floor. Perhaps the most significant result presented in this paper is the sub-300 ps FWHM CTR measured for 15 mm length BGO crystals with simple leading edge time pickoff at room temperature (see figures 2 and 3). An important note is that 15 mm length BGO crystals have ~6% higher photoelectric absorption probability for 511 keV photons compared to 20 mm LSO/LYSO crystals (Humm *et al* 2003). Therefore, these results are directly relevant to practical detector design for clinical PET systems. Furthermore, the 277 $\pm$ 7 ps FWHM CTR measured in this work is not simply due to the 15 mm crystal length. As an example, Brunner and Schaart (2017) showed a ~380 ps FWHM CTR at room temperature with 12 mm length BGO crystals. The improved CTR shown in this work results from the light readout sensor and improved single photon time resolution with the bootstrapping circuit readout.

As has also been shown in other work, a Lorentzian function provided the best fit to the CTR distributions, and the distributions have tails that extend beyond a standard Gaussian

kernel for CTR (see figures 4 and 5). In Brunner and Schaart (2017), it was shown that these tails manifest from the influence of BGO's luminescence on the timing estimator. While BGO does have a relatively fast luminescence component, it has poor light yield. Therefore, there can be large variance in the detection time of luminescence signatures from normal de-excitation processes, and this variance will influence the accuracy of the estimator for 511 keV photon time of interaction. For analog SiPMs, like those used in this work, leading edge timing estimators work as averaging estimators of the first n light photons (Gundacker *et al* 2015). The temporal variance of luminescence photons arriving within the same time frame as Cherenkov photons, within the earliest portion of the signal's rising edge (the first hundreds of picoseconds), contributes to error in the estimation of 511 keV photon time of interaction. This issue could be further combatted by boosting the detection efficiency for Cherenkov light, to minimize the influence of luminescence light's weighting on timing estimators. Along this direction, three immediately available approaches to improve results in the future are dual-sided readout of scintillation crystal elements (Seifert and Schaart 2015), coupling sensors along the long sides of long and narrow crystals (side readout) (Cates and Levin 2018b), or increasing SiPM photon detection efficiency deeper in the UV spectrum.

We presented analysis of the CTR distributions, regarding the influence of the observed tails on coincidence timing window beyond the standard Gaussian timing kernels. For all crystal lengths, >90% of coincidence events fall within a two nanosecond coincidence time window (figure 4). This is an important finding. If a substantial percentage of events within the CTR distribution fall outside of a standard timing window, then these events are lost, resulting in an effect drop in system sensitivity. Opening up the coincidence time window to captures these 'lost' events would increase a system's 'randoms' rate and negatively impact its noise equivalent count rate. The FWTM of distributions for the 3,5,10, and 15 mm length crystals in coincidence were 593 ± 14, 648 ± 12, 794 ± 25, 855 ± 23 ps (figure 3). When comparing Lorentzian and Gaussian curve fits to the 15 mm length crystal CTR distribution, only 17.7% of counts fell outside the full width of a standard Gaussian timing kernel (figure 5). These additional details on the measured CTR distribution are also important findings. A low percentage of events lying outside the bounds of a standard kernel indicates the signal-to-noise-ratio (SNR) improvements from TOF image reconstruction are not lost to weighting the 511 keV photon origin probability far outside the standard kernel, along the detector element lines of response. Since the focus of this work was to describe achievable CTR with this electronic readout technique applied to analog SiPMs coupled to BGO scintillators, we make quantitative comparisons between the observed CTR distributions and standard Gaussian fits to the data. However, detailed analyses that quantify how the shape of the distributions is related to and affects final reconstructed image SNR is beyond the scope of this work and will be investigated in future work.

In sections 3.1 and 3.2, we present CTR obtained with leading edge timing estimators with digital baseline correction, as the first goal was simply to measure what was achievable. Signal processing techniques that optimize timing channels for simple leading edge discriminators can reduce signal amplitude by removing the slow components of the signal. Since the circuits tested in this work improve SPTR essentially by boosting SNR, it was conceived that this might also affect CTR. As shown in figure 6, a balance can be struck for

the high pass filtering. Time constants that are too low will reduce signal amplitude such that the optimum leading edge threshold is no longer above noise. Filter constants that are too high do not adequately compensate for baseline shifts from high number of dark pulses and cross talk events at the overvoltages necessary to achieve the CTR values demonstrated in section 3. Interestingly, tuning the filter time constant can provide nearly the same CTR using a simple leading edge discriminator as the case when no filter is used with digital baseline compensated leading edge time pickoff.

The CTR values measured in this work are comparable to that achieved by state-of-the-art commercial TOF-PET systems, which are currently 214–400 ps FWHM (Hsu *et al* 2017, Philips 2019, Siemens 2019). Each of those systems employ detector modules comprising lutetium-based scintillation crystals. It is feasible that BGO-based TOF-PET detector modules could be developed with sub-300 ps FWHM with careful attention to multiplexing schemes that do not degrade timing performance. Such detector modules could be used to make TOF-PET systems having state-of-the-art CTR with a 4–5-fold lower scintillation material cost. They are also an attractive avenue to make total-body PET systems Cherry *et al* (2017) more economical.

5. Conclusions

We have reported achievable CTR for BGO crystals of various lengths using a readout technique that minimizes the influence of electronic noise on SPTR of large area, analog SiPMs. CTR between 200 ± 3 and 277 ± 7 ps FWHM was measured for crystal lengths ranging from 3–15 mm with leading edge time pickoff and room temperature operation. Therefore, the results presented here demonstrate that BGO crystals in combination with UV sensitive SiPMs and appropriate signal processing allow for PET detectors with CTR equivalent to what is currently state-of-the-art TOF-PET detector modules with 4–5-fold lower scintillation material cost.

Acknowledgments

This work was supported in part by NIH R01-CA214669-02 and R01-EB025125-02. The authors would like to thank Stefan Gundacker for the interesting discussions on this electronic readout. The authors would also like to thank Alberto Gola of Fondazione Bruno Kessler for providing the NUV-HD SiPMs used in this work.

References

Brunner SE and Schaart DR 2017 BGO as a hybrid scintillator / Cherenkov radiator for cost-effective time-of-flight PET Phys. Med. Biol 62 4421–39 [PubMed: 28358722]

Cates JW, Vinke R and Levin CS 2015 Analytical calculation of the lower bound on timing resolution for PET scintillation detectors comprised of high-aspect-ratio crystal elements Phys. Med. Biol 60 5141–61 [PubMed: 26083559]

Cates JW and Levin CS 2016 Advances in coincidence time resolution for PET Phys. Med. Biol 61 2255–65 [PubMed: 26914187]

Cates JW, Gundacker S, Auffray E, Lecoq P and Levin CS 2018a Improved single photon time resolution for analog SiPMs with front end readout that reduces influence of electronic noise Phys. Med. Biol 63 185022 [PubMed: 30129562]

Cates JW and Levin CS 2018b Evaluation of a clinical TOF-PET detector design that achieves ≤100 ps coincidence time resolution Phys. Med. Biol 63 115011 [PubMed: 29762136]

Cherry et al. 2017 Total-Body PET: maximizing sensitivity to create new opportunities for clinical research and patient care J. Nucl. Med 59 3–12 [PubMed: 28935835]

Gola A, Piemonte C and Tarolli A 2013 Analog circuit for timing measurements with large area SiPMs coupled to LYSO crystals IEEE Trans. Nucl. Sci 60 1296–302

Gundacker S, Auffray E, Frisch B, Jarron P, Knaptisch A, Meyer T, Pizzichemi M and Lecoq P 2013 Time of flight positron emission tomography towards 100 ps resolution with L(Y)SO: an experimental and theoretical analysis J. Instrum 8 P07014

Gundacker S, Auffray E, Pauwels K and Lecoq P 2016a Measurement of intrinsic rise times for various L(Y)SO and LuAG scintillators with a general study of prompt photons to achieve 10 ps in TOF-PET Phys. Med. Biol 61 2802–37 [PubMed: 26982798]

Gundacker S, Acerbi F, Auffray E, Ferri A, Gola A, Nemallapudi MV, Paternoster G, Piemonte C and Lecoq P 2016b State of the art timing in TOF-PET detectors with LuAG, GAGG, and L(Y)SO scintillatorsof various sizes coupled to FBK-SiPMs J. Instrum 11 P08008

Gundacker S, Auffray E, Jarron P and Lecoq P 2015 On the comparison of analog and digital SiPM readout in terms of expected timing performance Nucl. Instrum. Methods A 787 6–11

Hsu DFC, Ilan E, Peterson WT, Uribe J, Lubberink M and Levin CS 2017 Studies of next-generation silicon photomultiplier-based time-of-flight PET/CT system J. Nucl. Med 58 1511–8 [PubMed: 28450566]

Humm JL, Rosenfel A and Guerra AD 2003 From PET detectors to PET scanners Eur. J. Nucl. Med. Mol. maging 30 1574–97

Kwon SI, Gola A, Ferri A, Piemonte C and Cherry SR 2016a Bismuth germinate coupled to near ultraviolet silicon photomultipliers for time-of-flight PET Phys. Med. Biol 61 L38–L47 [PubMed: 27589153]

Kwon I, Kang T, Wells BT, D'Aries LJ and Hammig MD 2015 Compensation of the detector capacitance presented to charge-sensitive preamplifiers using the Miller effect Nucl. Instrum. Methods A 784 220–5

Kwon I, Kang T and Hammig MK 2016b Experimental validation of charge-sensitive amplifier configuration that compensates for detector capacitance IEEE Trans. Nucl. Sci 63 1202–8

Lecoq P, Korzhik M and Vasiliev A 2014 Can transient phenomena help improving time resolution in scintillators IEEE Trans. Nucl. Sci 61 229–34

Lecoq P 2017 Pushing the limits in time-of-flight PET imaging IEEE Trans. Radiat. Plasma Sci 1 473–85

Liu Z, Gundacker S, Pizzichemi M, Ghezzi A, Auffray E, Lecoq P and Paganoni M 2016 In-depth study of single photon time resolution for the Philips digital silicon photomultiplier J. Instrum 11 P06006

MACOM MABA-007159 Data Sheet. 2019. cdn.macom.com/datasheets/MABA-007159-000000.pdf

Minicircuits MAR-6 RF Amplifier Data Sheet. 2019. minicircuits.com/pdfs/MAR-6+.pdf

Philips Vereos PET/CT. 2019. usa.philips.com/healthcare/product/HC882446/vereos-digital-petct-provenaccuracy-inspires-confidence#galleryTab=360

Piemonte C, Acerbi F, Ferri A, Gola A, Paternoster G, Regazzoni V, Zappala G and Zorzi N 2016 Performance of NUV-HD Silicon Photomultiplier Technology IEEE Trans. Electron Devices 63 1111–6

Schaart DR, Seifert S, Vinke R, van Dam HT, Dendooven P, Lohner H and Beekman FJ 2010 LaBr3:Ce and SiPMs for time-of-flight PET: achieving 100 ps coincidence resolving time Phys. Med. Biol 55 N179–89 [PubMed: 20299734]

Siemens Biograph Vision PET/CT. 2019. usa.healthcare.siemens.com/molecular-imaging/pet-ct/biograph-vision

Seifert S, Vinke R, van Dam HT, Lohner H, Dendooven P, Beekman FJ and Schaart DR 2009 Ultra precise timing with SiPM-based TOF PET scintillation detectors NSS/MIC: IEEE Nuclear Science Symp. Conf. Record (Orlando) pp 2329–33

Seifert S and Schaart DR 2015 Improving the time resolution of TOF-PET detectors by double-side readout IEEE Trans. Nucl. Sci 62 3–11

Vinke R, Seifert S, Schaart DR, Schreuder FP, de Boer MR, van Dam HT, Beekman FJ, Lohner H and Dendooven P 2009 Optimization of digital time pickoff methods for $LaBr_3$-SiPM TOF-PET detectors NSS/MIC: IEEE Nuclear Science Symp. Conf. Record (Orlando) pp 2962–8

Zhang N and Schmand MJ 2016 Bootstrapping readout for large terminal capacitance analog-SiPM based time-of-flight PET detector US Patent US2016/0327657

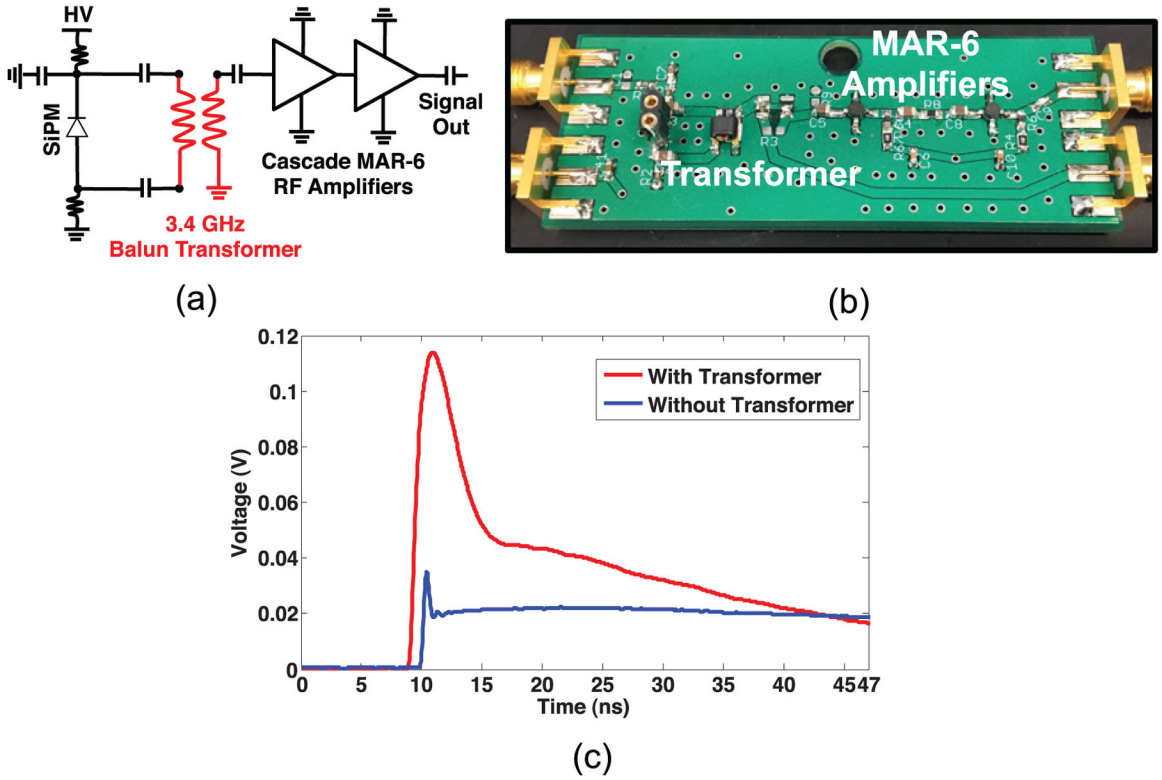

Figure 1.

The simplified schematic of a passive capacitance compensation circuit is shown in (a), and its implementation onto a PCB is shown in (b). In (c), the single average of 700 single photon pulses from a 3×3 mm^2 Hamamatsu S13360 SiPM is shown with and without the balun transformer in place (offset in time for clarity), for the circuit shown in (b) (Cates *et al* 2018a).

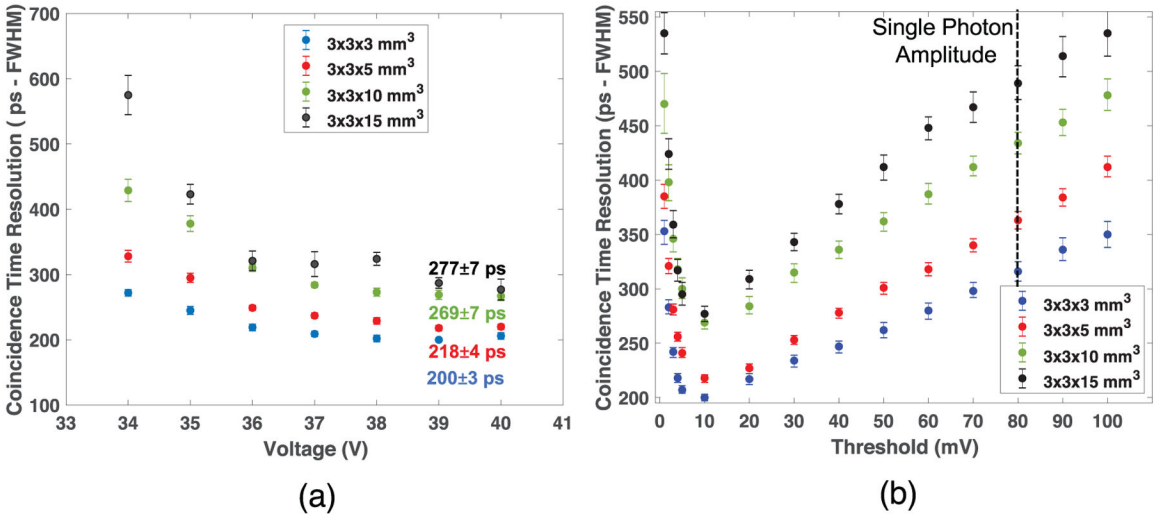

Figure 2.

Measured CTR at FWHM for BGO crystals with lengths varying from 3–15 mm versus applied voltage to SiPMs is shown in (a). In (b), CTR versus leading edge threshold is shown for each crystal length at the optimum applied SiPM bias.

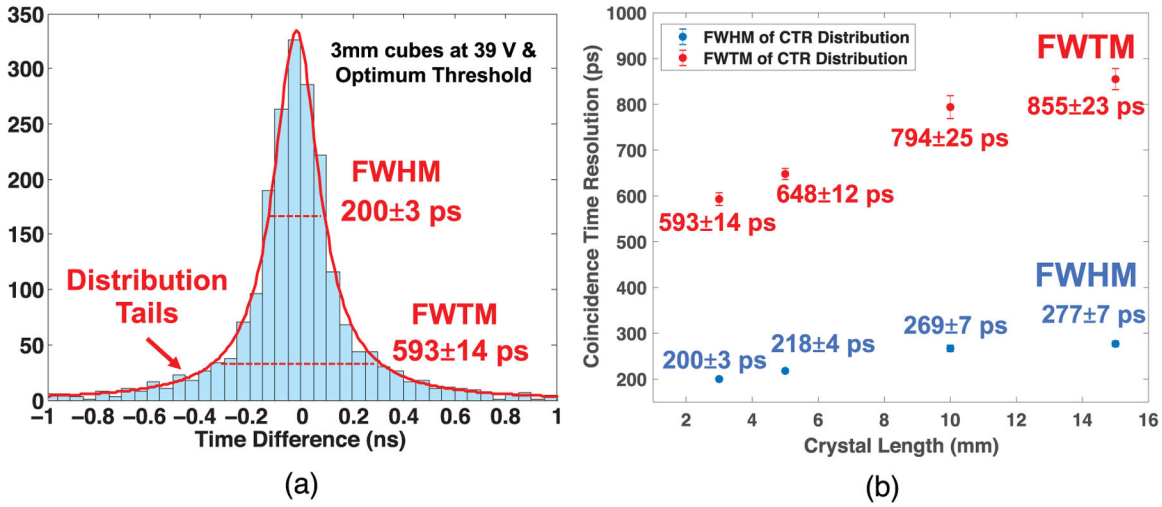

Figure 3.

CTR distribution for 3 × 3 × 3 mm^3 BGO crystals at optimum SiPM bias and leading edge threshold with a Lorentzian curve fit to the distribution. In (b), CTR at FWHM and FWTM of the distributions for 3–15 mm length crystals at optimum SiPM bias and leading edge threshold is plotted.

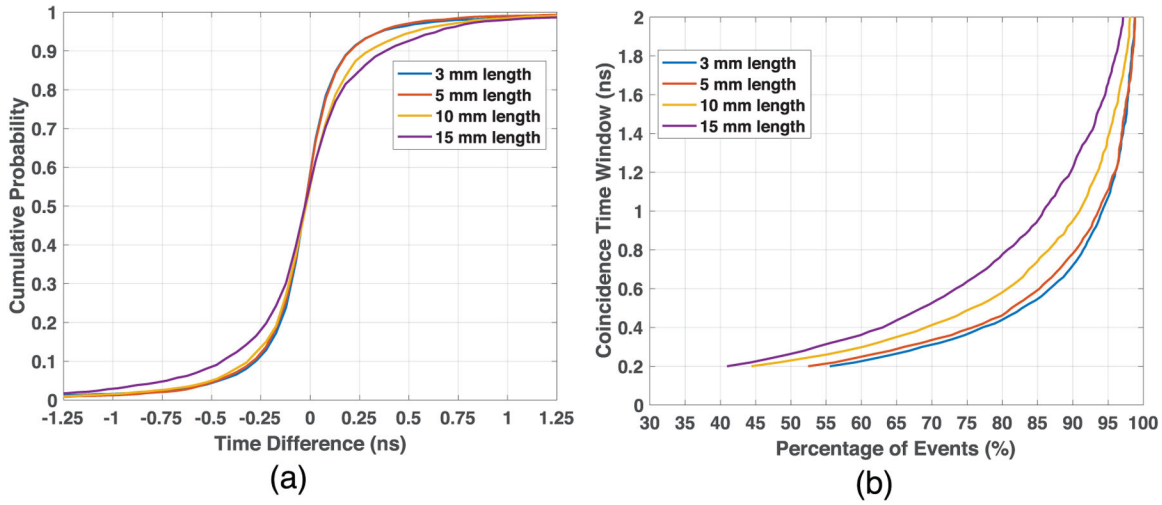

Figure 4.

Cumulative distribution curve for CTR distributions for 3–15 mm length crystals is shown in (a). In (b), the percentage of coincidence events falling within a set coincidence window is plotted for the crystals.

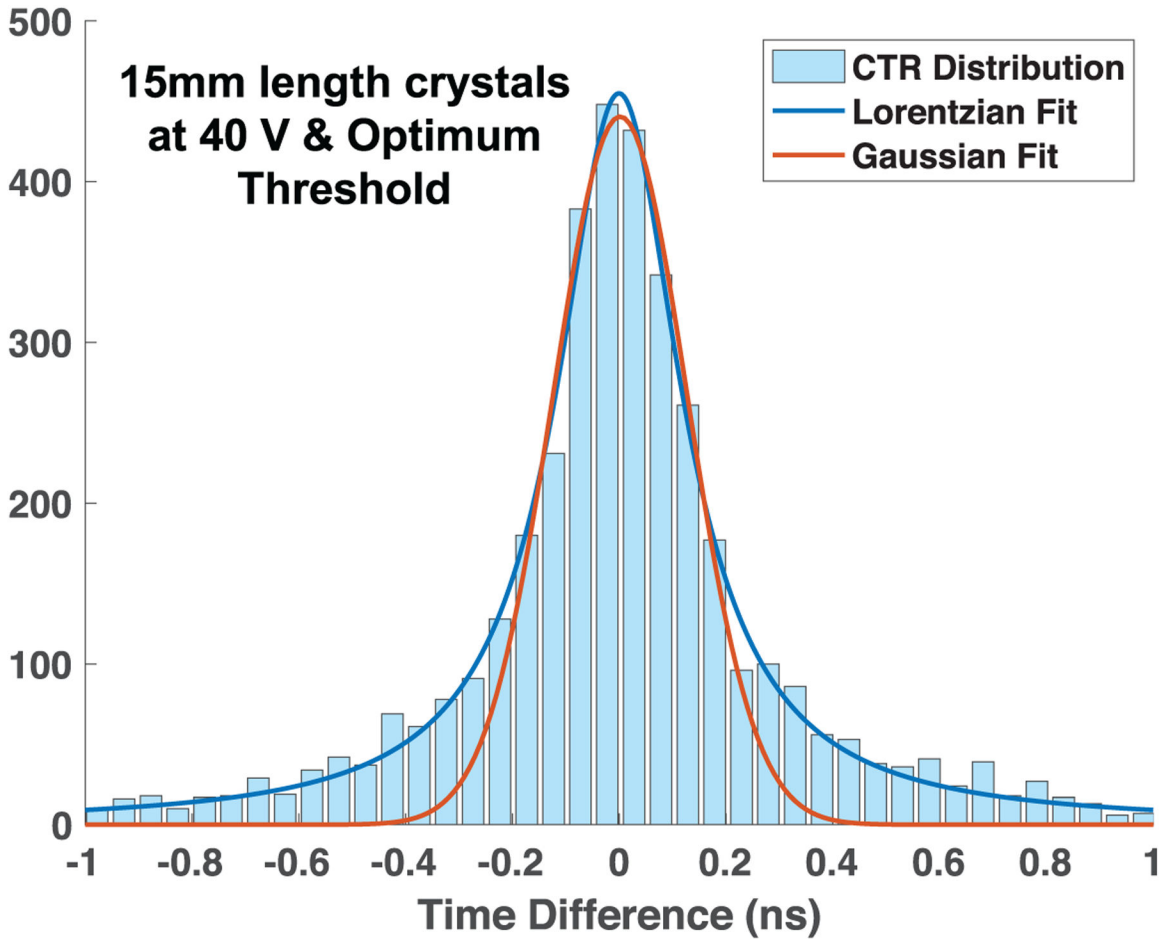

Figure 5.
CTR distribution for 15 mm length crystals with optimum SiPM bias and leading edge threshold with both Lorentzian and Gaussian curve fits is shown.

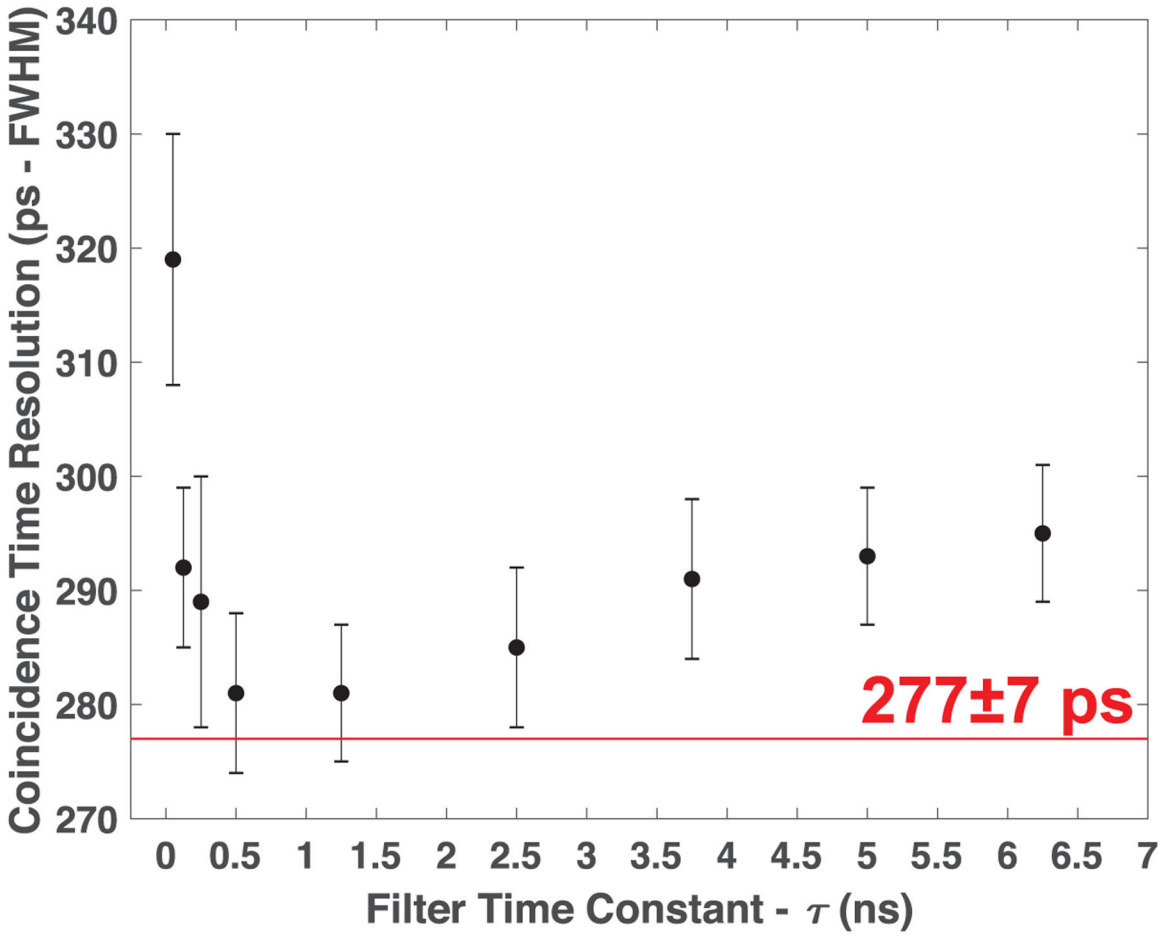

Figure 6.

CTR at FWHM for $3 \times 3 \times 15$ mm^3 with optimum SiPM bias and simple leading edge threshold is plotted versus high pass filter time constant applied to the digitized timing waveforms. The red line indicates the best CTR for the same data with digital baseline corrections employed.